Eurographics Workshop on Visual Computing for Biology and Medicine (2024)
L. Garrison and D. Jönsson (Editors)

Short Paper

Potential of Tetrahedral Markers for Infrared Pose Tracking in Surgical Navigation

Erik Immoor[1] and Tom L. Koller[1,2]

[1] University of Bremen, Germany
[2]Fraunhofer MEVIS, Germany

Abstract

Optical tracking systems predominantly rely on spherical retro-reflective markers, requiring a minimum of three fiducials to achieve a full six-degree-of-freedom (6D) pose estimation. Despite the potential benefits of a single non-spherical fiducial for 6D pose estimation, this approach has received limited attention in the literature. This study investigates the feasibility of non-spherical retro-reflective markers, specifically tetrahedral markers, as alternatives to spherical fiducials. Using Blender for simulation and digital post-processing, stereo images of both spherical and tetrahedral markers were generated. The standard marker tracking is adapted to use the tetrahedrons corners instead of sphere centers. Results indicate that while spherical markers provide slightly more precise tracking in the simulated scenario, tetrahedral markers offer advantages in practical applications, such as an enhanced range of motion. These findings suggest that non-spherical markers warrant further exploration for their potential to improve optical tracking systems in real-world settings.

CCS Concepts

• ***Computing methodologies*** → ***Tracking;*** *Epipolar geometry;*

1. Introduction

Retro-reflective markers are integral to optical tracking systems in medical applications [GSH11, SPM*20, GLP*21]. These markers enable precise localization and tracking of patients and medical instruments during surgical procedures, such as minimally invasive operations. The implementation of these markers enhances operational efficiency, mitigates intervention risks and pain, and shortens hospital stays [SPM*20]. Generally, spherical fiducials are used due to their consistent appearance from all viewing angles and easy tracking. However, markers with spherical fiducials also present significant drawbacks, including self-occlusion, problematic reflections [WLY*19, SPM*20], and the creation of ghost markers [LYZ*18]. These issues can compromise the accuracy and reliability of tracking. In particular, self-occlusion burdens the surgeon as it reduces the range of visibility and forces the surgeon to orientate the instrument more thoroughly towards the camera.

Spherical fiducials occlude each other when their 2d projections are touching or overlapping in the 2D image. The center of gravity of the spheres cannot be reliably detected as a feature in these cases. When the number of detectable features reduces below 3, the marker cannot be tracked. To circumvent this, we propose to use a fiducial that has at least 3 features in itself that are not subject to self-occlusion. To the best of our knowledge, no study exists that evaluates fiducials with 3 or more features. Non-spherical fiducials are either lenticular fiducials [NDI24b], which, like a sphere, describe only one point, or markers for specialized applications, such as tracking scissors [Pen05] with retroreflective lines or people [CZKD19] with straps and patches.

In this preliminary study, we evaluate the suitability of a tetrahedral marker as an example for a non-spherical fiducial with 4

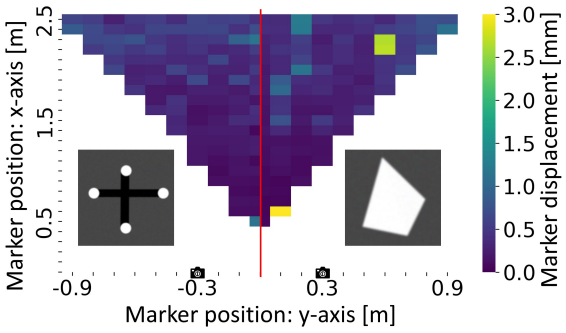

Figure 1: *Average deviation of the marker positions in a split heat map in mm. Left: spherical marker. Right: tetrahedral marker. The camera positions are marked. Deviations are averaged over z-axis.*

DOI: 10.2312/vcbm.20241184

features for optical tracking. We choose the tetrahedron due to its triangle faces. In current infrared tracking, feature positions are converted from 2D pixels positions on images from two cameras via epipolar geometry. Due to the triangle faces, 3 features are visible in both cameras simultaneously from most angles. We conduct a comparative analysis on simulated images to determine whether non-spherical markers can deliver the expected benefits in practical applications and whether they achieve the required accuracy for surgical applications (see Figure 1). [WLY*19]

2. Methodology

In this study, we adapt a standard pipeline [ZWD*17, GSH11, WLY*19] for spherical marker tracking to a tetrahedral marker. We use the term "spherical marker" to name a marker geometry with 4 spheres as fiducials. The stereo image data is generated in a simulation environment, since it provides the exact ground truth of the marker poses. The whole Pipeline can be seen in Figure 2. We use Blender [Ble24] with the VisionBlender add-on [CTL*21] to simulate stereo images of spherical and tetrahedral retro-reflective markers and generate the ground truth. To mimic simple real-world effects, we apply post-processing techniques to introduce noise, distortion, and blurring. The parameters of the image generation are listed in the Table 3 in the Appendix.

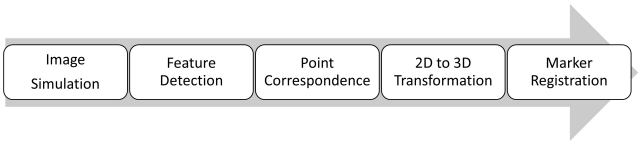

Figure 2: *Steps of the marker tracking pipeline.*

For spherical markers we re-implement the tracking approach in [Suz85]. The sphere centers are extracted by finding the centers of gravity of the contours. Point correspondence between the stereo images is established using epipolar lines and the 3d positions of the markers are computed via stereo geometry. The marker registration is performed using the least squares method to minimize positional discrepancies [AHB87, Kan94]. The marker tracking is implemented in Python using OpenCV.

The pipeline for spherical marker tracking can be adapted to track tetrahedral markers by exchanging the feature extraction. Instead of the sphere centers, the corners of the tetrahedral marker are used as features (see Figure 3). These are detected with the Shi-Tomasi corner detector [JT94] and refined with the Förstner algorithm [FG87]. We choose this approach for its simplicity, availability of the algorithms in public libraries and similarity to the standard methodology. As long as 3 features of the marker are visible in both images, the remaining pipeline for point correspondences and marker registration stays unmodified.

The spherical marker is based on a design from NDI [NDI24a], a leading provider of optical tracking systems. Since the tetrahedral marker spans the features in 3D rather than on a 2D plane, it is unknown how to design the geometry so that it is comparable in terms of the expected marker pose accuracy under the assumption that the feature detection accuracy would be equal. We choose a

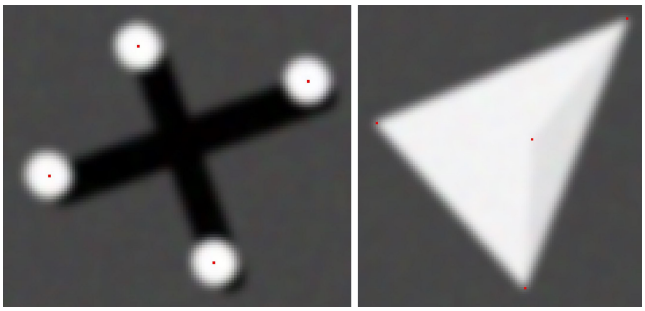

Figure 3: *Image section of spherical and tetrahedral markers with marked pixels of the features.*

tetrahedron which base triangle has the same extent as the bounding box of the spherical marker (see Figure 4). Thus, they are similar in the maximum distances of features.

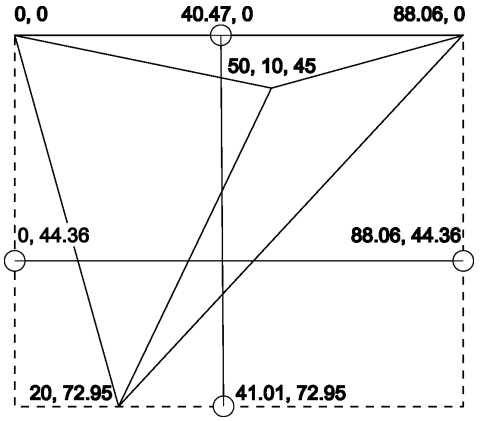

Figure 4: *Marker geometries overlayed. The dashed line shows the bounding box of the spherical marker. All coordinates in mm.*

Furthermore, the features of the tetrahedral marker are positioned so that their pairwise distances are unique to allow feature correspondence. In contrast to the NDI guidelines [NDI21] we choose a minimum of 6mm difference for uniqueness. A visual size comparison is shown in Figure 5.

By maintaining a consistent processing pipeline for both marker shapes, except for the initial feature detection step, we ensured the results are not skewed due to different methods in the pipeline. This approach allows us to evaluate the feasibility and advantages of non-spherical markers in optical tracking systems.

3. Results

The following results are based on a comprehensive set of 1941 image pairs for both spherical and tetrahedral markers. While rotating, the markers move in ten-centimeter increments within the cameras field of view, ranging from a distance of 0.5 m to 2.5 m. The tetrahedral marker is rotated around all 3 world axes. The spherical marker is only rotated around its normal axis (in plane rotation) which is chosen to prevent self-occlusion in the first experiment. This setup

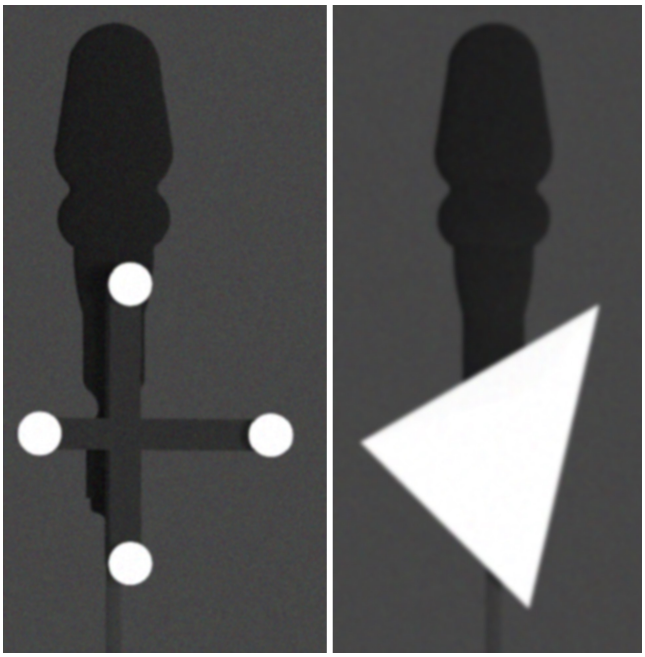

Figure 5: *Comparision of the spherical and tetrahedral markers mounted at an awl in identical image sections.*

was designed to replicate the conditions of commercial tracking systems. First, we evaluate the feature detection and marker pose on this dataset followed by an analysis of the view angle on a specialized dataset.

3.1. Feature Detection

The precision of feature detection varies strongly between the two marker shapes. The center detection for the spherical markers has an average error of 0.14 ± 0.08 px (standard deviation) . This level of accuracy was consistent across the entire range of distances of the image set. In contrast, the corner detection for tetrahedron-shaped markers has an average error of 0.30 ± 0.16 px. Since the tracking accuracy depends on the distance to the camera, the average errors for 4 distances categories can be seen in Table 1. The transitions between categories is mostly smooth. Notably, the accuracy of detection for the corner features decreased as the markers moved closer to the cameras. The reason for this behavior is unknown.

Table 1: *Average errors for different distance sections. Pixel error of the feature detection, position error and rotation error.*

distance	0.5-1.0 m	1.0-1.5 m	1.5-2.0 m	2.0-2.5 m
sph. feature	0.13	0.10	0.13	0.16
tet. feature	0.62	0.41	0.30	0.25
sph. position	0.41	0.22	0.40	0.62
tet. position	0.53	0.22	0.40	0.67
sph. rotation	0.76	0.23	0.77	1.53
tet. rotation	0.91	0.35	0.60	1.6

3.2. Marker Pose Tracking

The results of the feature recognition directly influence the outcomes of the marker tracking. As anticipated, tracking errors of the center position for both spherical and tetrahedral markers increase with distance from the cameras (see Table 1). The reason for this is the inversely proportional relationship of distance and disparity. The only exception is a high error in the closest region. This is mainly due to features being cut-off by the image borders since they appear larger. The average error is 0.49 ± 0.77 mm for the spherical marker and 0.53 ± 1.70 mm for the tetrahedral marker. This greater deviation is the result of the less precise feature detection. Additionally, incorrect marker registrations occasionally occur with the tetrahedral markers which causes the high standard deviation.

While the displacement of markers during tracking is a crucial error variable, the rotation error is equally important, especially when using the marker to infer the position of a distant point like the tip of a tool. Following [HWFS13], we define the rotation error as the angle of the smallest rotation which rotates the tracked marker to the ground truth. In this study, the distribution of the rotation error is comparable to the displacement (see Table 1). The average rotation error is $1.11 \pm 1.72^\circ$ for the spherical marker and $1.12 \pm 7.81^\circ$ for the tetrahedral marker. The tetrahedral marker performs worse in close distance (0.5-1.0 m) and better at a distance of 1.5-2.0 m.

A decisive factor in marker tracking is the number of features used for tracking. The tetrahedron-shaped marker is designed with four corner points that can be localized as features. However, in the image set used for this study, only three features could be localized in 91.5% of cases. Remarkably, we observe that the marker pose has a higher error with more visible features (see Table 2). Apparently, the feature detection error increases when all 4 features are visible.

Table 2: *Comparison of the average values of the feature deviation, marker displacement and rotation error for three and four localized features*

	3 features	4 features	spherical
feature deviation	0.28 px	0.38 px	0.14 px
displacement	0.53 mm	0.54 mm	0.50 mm
rotation error	0.98°	2.12°	1.11°

3.3. View Angle

For an analysis of the viewing area we use two additional data sets, each containing 180 images. In these sets, the markers are mounted on an awl positioned centrally at a distance of 1 m from the cameras. Initially, the marker is oriented directly towards the cameras, and with each successive image, the awl rotates one degree clockwise around the instruments longest axis (see Figure 6). This analysis reveals that the tetrahedral marker offers a larger viewing area for tracking. In this case it amounts to approximately 30° more than the spherical marker. Specifically, the tracking error of the spherical marker increases vastly above 60° whereas the accuracy of the tetrahedron shaped marker stays approximately constant until 90°. The cutoff for the spherical markers is only exemplary as the angle

where the spheres start to overlap depends on the marker geometry and the axis of rotation.

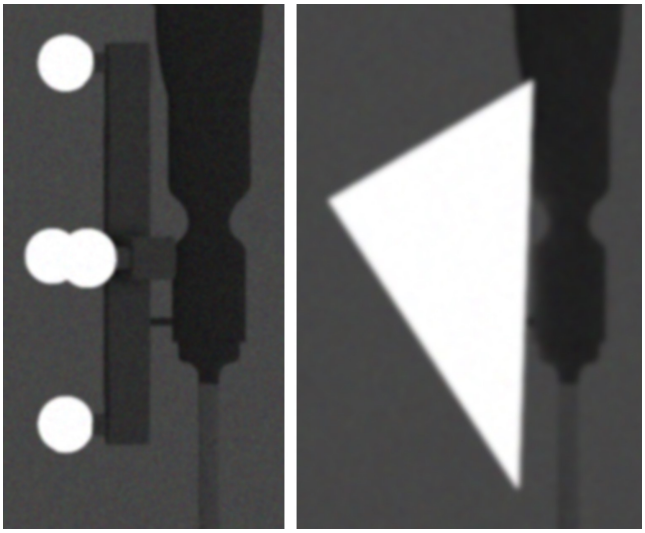

Figure 6: *Spherical and tetrahedral markers mounted at an awl which is rotated at 90°.*

4. Discussion

In principle, the spherical marker enables more precise tracking than the tetrahedron-shaped marker, provided that all four spheres are visible. The reason for this is the smaller errors in feature recognition, which affect the entire tracking process.

4.1. Feature Detection

The results of the feature detection clearly show that the spherical features can be tracked with higher accuracy. The errors for the tetrahedral marker are on average around two times as large. While the spherical center is calculated based on all pixels of the contour, each corner is only calculated based on a small window surrounding the corner. This means that the feature detection for spherical markers is based on a larger number of pixels and therefore achieves smaller errors. One way to tackle this problem could be to use the edges to calculate the corner points [GVGJMR12].

The lower feature detection accuracy is the reason why we choose 6 mm as difference between pair-wise feature distances in the tetrahedral marker in contrast to the 3 mm NDI suggests [NDI21]. A smaller difference causes mismatches of the features correspondences which results in large pose errors. During marker design, we also observed that the corner shape (e.g. its angles) influence the feature detection. This coincides with the increased feature detection error when all features are visible. The corner detection appears to vary greatly between perspectives and shapes. This has to be investigated systematically.

4.2. Marker pose estimation

The error of the pose estimation of the tetrahedral marker is only slightly higher compared to spherical marker. The standard deviation of the tetrahedral marker is much higher. This shows, that the marker is in principle suited for medical tracking applications, but the current feature detection method is highly unstable.

In 91.5% of the images, only 3 of the tetrahedrons corner features are visible. That is a systematic drawback of the tetrahedral shape compared to the 4-sphere marker, since the accuracy usually increases with the number of visible features [SPM*20]. Unfortunately, this appears to be a property of tetrahedral shaped markers, since the fourth feature is not visible in infrared whenever it is behind or in front of a triangle plane. Thus, tetrahedral shapes are sub-optimal to achieve high pose accuracy. This also means that the tetrahedral marker is effectively self-occluding which we aimed to eliminate. However, the occlusion is qualitatively different as it still allows 3 features to be tracked. In contrast, two touching spherical markers result in an average marker position with a high error. This error prevents to match the features to the marker geometry.

The tetrahedral marker design is rather large for a surgical instrument and could be a hindrance to the surgeon. The size of the marker has to be chosen in a trade-off with the accuracy.

Overall, tetrahedral markers show promising accuracy. Due to the 3D shape, they are bulky, when they have the same feature distance as standard 4-sphere markers. Their corner features are harder to track with high pixel accuracy and less features are visible from most perspectives. Their advantage is a higher range of visibility under rotations, due to their robustness against self-occlusions.

4.3. Simulation Reality Gap

One of the major advantages of infrared tracking with retro-reflective markers is the simple image processing to segment the markers in the image. Real world challenges like varying lightning conditions, different environments and challenging background objects are much less severe than in RGB based tracking. Hence, we expect the simulation reality gap to be less pronounced than in applications like machine learning. However, multiple challenges arise in the clinical setting which have not been adressed by the current evaluation of the tetrahedral marker. Namely occlusions, pollution, overlaps and reflections. Finally, the production of the actual markers must also be examined.

Occlusion occurs, when other objects or humans break the line of sight between the markers and the camera. Another source of marker occlusion is pollution. The retro-reflective material can loose its reflective properties when it is stained with blood, fat or other liquids. In the simulation, we only use single markers and no metal reflections occur. In the real setup, these effects can hinder the accurate detection of features, as markers may overlap with each other or reflections. Sphere markers allow to detect partial occlusion and reflections. Both effects can be detected from the size and roundness of the marker projection and the pose can still be estimated as long as 3 spheres are visible. It has to be tested, whether occlusion and overlaps can be safely detected for tetrahedral markers. Since most of the times only 3 features are visible, we expect tetrahedral markers to be prone to these effects. A single hidden feature causes the tracking to fail.

5. Conclusion

In this simulation study, the tetrahedral marker has performed slightly worse than the spherical marker. The corner detection is less precise than the center detection for spherical markers and the shape itself only allows to track 3 features from most perspectives. This results in an average position error of 0.53 mm and rotation error of 1.12°. We have demonstrated that the tetrahedron can enlarge the usable field of view by 30° in comparison to the spherical marker, which improves usability. Therefore, the marker concept is promising for navigated surgery.

Future research should explore how to improve and stabilize the tracking accuracy. Given the current limitations in corner point detection, it is crucial to investigate alternative methods for feature recognition to achieve higher accuracy. Exploring other non-spherical shapes could offer promising solutions. As shown, the tracking accuracy can be improved if more than 3 features are visible. Since most of the time only 3 features of the tetrahedral markers are visible, other shapes like hexahedrons have to be explored. To track these, it might be required to deviate from the classic approach to use corresponding pairs of features in the images.

References

[AHB87] ARUN K. S., HUANG T. S., BLOSTEIN S. D.: Least-squares fitting of two 3-d point sets. *IEEE Transactions on Pattern Analysis and Machine Intelligence PAMI-9*, 5 (Sept. 1987), 698–700. doi:10.1109/TPAMI.1987.4767965. 2

[Ble24] BLENDER FOUNDATION: blender.org - home of the blender project - free and open 3d creation software, 2024. URL: https://www.blender.org/. 2

[CTL*21] CARTUCHO J., TUKRA S., LI Y., S. ELSON D., GIANNAROU S.: VisionBlender: a tool to efficiently generate computer vision datasets for robotic surgery. *Computer Methods in Biomechanics and Biomedical Engineering: Imaging & Visualization 9*, 4 (July 2021), 331–338. doi:10.1080/21681163.2020.1835546. 2

[CZKD19] CHATZITOFIS A., ZARPALAS D., KOLLIAS S., DARAS P.: DeepMoCap: Deep optical motion capture using multiple depth sensors and retro-reflectors. *Sensors 19*, 2 (Jan. 2019), 282. arXiv:2110.07283[cs], doi:10.3390/s19020282. 1

[FG87] FÖRSTNER W., GÜLCH E.: A fast operator for detection and precise location of distinct points, corners and circular features. In *Proceedings of the Intercommission Conference on Fast Processing of Photogrammetric Data* (June 1987). Place: Interlaken. 2

[GLP*21] GSAXNER C., LI J., PEPE A., SCHMALSTIEG D., EGGER J.: Inside-out instrument tracking for surgical navigation in augmented reality. In *Proceedings of the 27th ACM Symposium on Virtual Reality Software and Technology* (Aug. 2021), ACM, pp. 1–11. Place: Osaka Japan. doi:10.1145/3489849.3489863. 1

[GSH11] GARCIA E., SÜLTROP C., HAUSOTTE T.: Verbesserung der detektion sphärischer marker für die optische navigationschirurgie. In *Proceedings of CURAC 2011* (Sept. 2011). 1, 2

[GVGJMR12] GROMPONE VON GIOI R., JAKUBOWICZ J., MOREL J.-M., RANDALL G.: LSD: a line segment detector. *Image Processing On Line 2* (Mar. 2012), 35–55. doi:10.5201/ipol.2012.gjmr-lsd. 4

[HWFS13] HERTZBERG C., WAGNER R., FRESE U., SCHRÖDER L.: Integrating generic sensor fusion algorithms with sound state representations through encapsulation of manifolds. *Information Fusion 14*, 1 (Jan. 2013), 57–77. doi:10.1016/j.inffus.2011.08.003. 3

[JT94] JIANBO SHI, TOMASI: Good features to track. In *Proceedings of IEEE Conference on Computer Vision and Pattern Recognition CVPR-94* (1994), IEEE Comput. Soc. Press, pp. 593–600. Place: Seattle, WA, USA. doi:10.1109/CVPR.1994.323794. 2

[Kan94] KANATANI K.: Analysis of 3-d rotation fitting. *IEEE Transactions on Pattern Analysis and Machine Intelligence 16*, 5 (May 1994), 543–549. doi:10.1109/34.291441. 2

[LYZ*18] LIN Q., YANG R., ZHANG Z., CAI K., WANG Z., HUANG M., HUANG J., ZHAN Y., ZHUANG J.: Robust Stereo-Match Algorithm for Infrared Markers in Image-Guided Optical Tracking System. *IEEE Access 6* (2018), 52421–52433. doi:10.1109/ACCESS.2018.2869433. 1

[NDI21] NDI - NORTHERN DIGITAL INC.: *Polaris Tool Design Guide*, R01 ed., Feb. 2021. 2, 4

[NDI24a] NDI - NORTHERN DIGITAL INC.: NDI passive spheres for IGS: Compatibility and precision, 2024. URL: https://www.ndigital.com/optical-navigation-technology/passive-marker-spheres/ndi-passive-sphere/. 2

[NDI24b] NDI - NORTHERN DIGITAL INC.: NDI radix lens: Wipeable retro-reflective lens, 2024. URL: https://www.ndigital.com/optical-navigation-technology/radix-lens/. 1

[Pen05] PENTENRIEDER K.: Tracking scissors using retro-reflective lines, Jan. 2005. URL: https://campar.in.tum.de/pub/pentenrieder2005da/pentenrieder2005da.pdf. 1

[SPM*20] SORRIENTO A., PORFIDO M. B., MAZZOLENI S., CALVOSA G., TENUCCI M., CIUTI G., DARIO P.: Optical and Electromagnetic Tracking Systems for Biomedical Applications: A Critical Review on Potentialities and Limitations. *IEEE Reviews in Biomedical Engineering 13* (2020), 212–232. doi:10.1109/RBME.2019.2939091. 1, 4

[Suz85] SUZUKI S.: Topological structural analysis of digitized binary images by border following. *COMPUTER VISION, GRAPHICS, AND IMAGE PROCESSING 30* (1985), 32–46. 2

[WLY*19] WU H., LIN Q., YANG R., ZHOU Y., ZHENG L., HUANG Y., WANG Z., LAO Y., HUANG J.: An Accurate Recognition of Infrared Retro-Reflective Markers in Surgical Navigation. *Journal of Medical Systems 43*, 6 (Apr. 2019), 153. doi:10.1007/s10916-019-1257-x. 1, 2

[ZWD*17] ZHOU Z., WU B., DUAN J., ZHANG X., ZHANG N., LIANG Z.: Optical surgical instrument tracking system based on the principle of stereo vision. *Journal of Biomedical Optics 22*, 6 (June 2017), 065005. doi:10.1117/1.JBO.22.6.065005. 2

6. Appendix

Table 3: *Parameters of the cameras in blender and other parameters that differ from the default value (first part of the table). Parameters for the post processing (second part of the table).*

parameter	value
focal length	8mm
sensor size	8.51mm
resolution	3072 x 2048
baseline	0.3m
stereoscopy mode	parallel
render engine	cycles
max samples	512
k1, k2, k3, p1, p2	0.5, 0.2, 0.1, 0, 0
Gaussian noise (μ, σ^2)	0, 0.001
Gaussian filter size	9 x 9